NANO LETTERS

LETTER

pubs.acs.org/NanoLett

High-Resolution Field Effect Sensing of Ferroelectric Charges

Hyoungsoo Ko,[†,‡] Kyunghee Ryu,[§] Hongsik Park,[†,∥] Chulmin Park,[†,‡] Daeyoung Jeon,[†,⊥] Yong Kwan Kim,[†,‡] Juhwan Jung,[†,‡] Dong-Ki Min,[†,‡] Yunseok Kim,[#] Ho Nyung Lee,[¶] Yoondong Park,[†,‡] Hyunjung Shin,[§] and Seungbum Hong[*,†,□]

[†]Semiconductor Device Laboratory, Samsung Advanced Institute of Technology, Yongin 446-712, Korea

[‡]Semiconductor R&D center, Samsung Electronics, Yongin 446-711, Korea

[§]School of Advanced Materials Engineering, Kookmin University, Seoul 136-702, Korea

[∥]Division of Engineering, Brown University, Providence, Rhode Island 02912, United States

[⊥]School of Electrical Engineering, Korea University, Seoul 136-713, Korea

[#]Max Planck Institute of Microstructure Physics, Halle (Saale) 06120, Germany

[¶]Materials Science and Technology Division, Oak Ridge National Laboratory, Oak Ridge, Tennessee 37831, United States

[□]Materials Science Division, Argonne National Laboratory, Lemont, Illinois 60439, United States

Supporting Information

ABSTRACT: Nanoscale manipulation of surface charges and their imaging are essential for understanding local electronic behaviors of polar materials and advanced electronic devices. Electrostatic force microscopy and Kelvin probe force microscopy have been extensively used to probe and image local surface charges responsible for electrodynamics and transport phenomena. However, they rely on the weak electric force modulation of cantilever that limits both spatial and temporal resolutions. Here we present a field effect transistor embedded probe that can directly image surface charges on a length scale of 25 nm and a time scale of less than 125 μs. On the basis of the calculation of net surface charges in a 25 nm diameter ferroelectric domain, we could estimate the charge density resolution to be as low as 0.08 μC/cm^2, which is equivalent to 1/20 electron per nanometer square at room temperature.

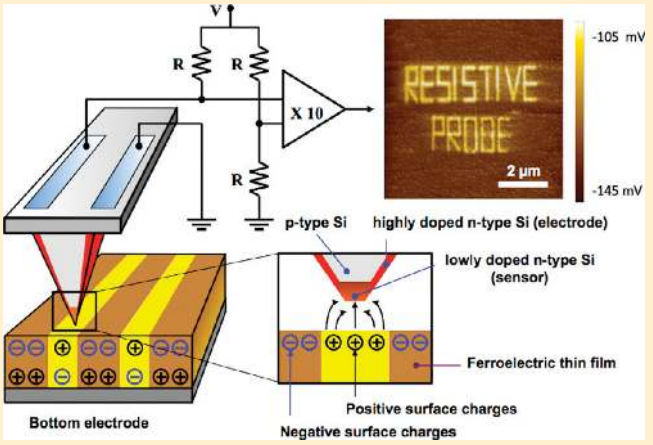

KEYWORDS: Charge imaging, field effect, resistive probe, ferroelectric, scanning probe microscopy

Various high-resolution SPM techniques are capable of probing local electrical,[1] magnetic,[2] chemical,[3] piezoelectric,[4] and thermal properties[5] of condensed and soft matters as well as manipulating these properties at the nanoscale.[6,7] Among those various techniques, electrostatic force microscopy (EFM) and Kelvin probe force microscopy (KFM) have been widely used to characterize the surface potential and electric field of ferroelectric surface,[8] DNA/protein arrays,[9] nanowires/nanotubes,[10] and trapped charges at the interfaces.[11] Since both EFM and KFM primarily detect a small change in cantilever deflection (on the order of subnanometers to a few nanometers) induced by the electric force, they are under strong influence of interferences by other forces, for example, van der Waals force, capillary force, and thermal energy fluctuations, which are acting on the tip or cantilever. Therefore, to minimize the nonlinear contribution from such forces, one needs to use a very stiff cantilever and maintain a certain gap between the tip and sample surface, which deteriorates the spatial resolution of both EFM and KFM. Furthermore, data acquisition speed is mainly limited by the mechanical resonance frequency of the cantilever or the modulation frequency of the lock-in amplifier.

For circumventing the spurious coupling with the cantilever motion, various direct charge imaging methods have been proposed and reported. For example, Yoo et al. reported the design and fabrication of a single-electron transistor tip to image individual surface charge distribution on a length scale of 100 nm at 4.2 K.[12] However, the low-temperature operation limits its practical applications. Suh et al. reported a field effect transistor (FET) probe fabricated on top of the silicon tip with a spatial resolution of about 300 nm.[13] The reason behind the poor resolution comes from the fact that the gate is defined after the tip is formed; thus, it is difficult to reduce the size of the sensing region and align it exactly onto the tip apex. Previously, we demonstrated the scanning resistive probe microscopy (SRPM) that has an electric field sensor aligned at the

Received: September 24, 2010
Revised: February 14, 2011
Published: March 04, 2011

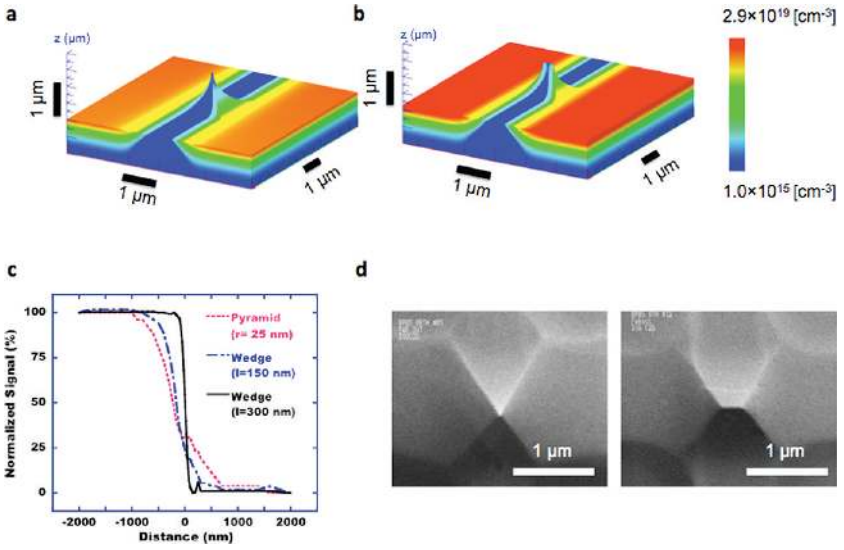

Figure 1. Simulated structures with dopant concentration distributions and estimation of spatial resolution. (a,b) Three-dimensional dopant concentration plots for point (a) and wedge shaped resistive probes (RPs) (b). (c) Plot of the simulated RP signal across positive and negative charge domains for point and wedge shaped probes. (d) Scanning electron microscopy images of point (left) and wedge-shaped probes (right).

tip apex with a spatial resolution of about 200 nm and a temporal resolution of 10 ns.[14,15] Like other methods described above, SRPM also suffered from the poor spatial resolution even though the position of sensor was aligned with the tip apex. Here we present our detailed analysis on the reasons for the poor spatial resolution of SRPM and an improved design of SRPM that has a wedge-shaped electric field sensor. The wedge-shaped resistive probe (RP) offers a far better spatial resolution without losing its high speed acquisition rate for detecting surface charges at room temperature down to 25 nm in lateral size.

Results and Discussion. For optimizing the process and improving the spatial resolution, we conducted both process and device simulations using technology computer-aided design (TCAD)[16] that build tip structures with various dopant profiles and measured the source−drain current as the tip moves across the oppositely charged electrodes, of which details can be found in Supporting Information. However, contrary to our prior expectation, we found that a geometrically sharper tip leads to a poorer spatial resolution of surface charge. The simulation results shown in Figure 1c clearly demonstrate a drastic improvement of the spatial resolution by changing the probe shape from pyramid to wedge. In addition, the resolution further improves as we increase the length of wedge from 150 to 300 nm. To better understand the underlying physics behind such an improvement, we compared the geometry and dopant concentration distribution of both pyramidal and wedge-shaped RPs as shown in Figures 1a,b, which illustrate the three-dimensional plots of the pyramidal and wedge-shaped RPs with dopant concentration distribution represented by color scale bars. On the basis of our structure and device analyses, we found three main reasons responsible for the improvement as follows: the volume of high sensitivity region (lowly doped region) becomes more spatially confined to a smaller region, the total resistance of the probe decreases as manifested by higher dopant concentration in the periphery regions around the tip, and the electric field gradient gets steeper. In other words, by preserving the highly doped region next to the lowly doped sensing region, we could form electric shields wrapping the sensor that reduced the contribution of parasitic electric fields outside the region of interest, and lower the total device resistance that contributed to higher sensitivity in terms of $\Delta R/R$.[17]

The source, channel, and drain regions were formed using a 300 keV As^+ implantation process with a stripe-shaped oxide implantation mask of which a portion was then used as an isotropic tip-etching mask, thereby making the channel area aligned with the tip apex.[18] To have a wedge shape instead of a sharp pyramidal tip, we varied the aspect ratio of tip mask and optimized the process for the desired shape and length (see Supporting Information). Figure 1d shows the comparative scanning electron microscopy (SEM) images of the pyramidal and wedge-shaped RPs.

Figure 2a−c shows the SRPM, KFM and PFM (phase) images of a selectively polarized region in an epitaxially grown $PbZr_{0.2}Ti_{0.8}O_3$ thin film on a $SrRuO_3/SrTiO_3$ substrate. On the basis of the PFM phase image in Figure 2c, we find that the bright contrast corresponds to domains with downward (negative) polarization whereas the dark contrast to those with upward (positive) polarization formed by local polarization switching. The corresponding PFM amplitude image (not shown here) confirms that both positive and negative domains are fully extended through the film thickness. PFM is known to be insensitive to topography and screen charges[19] and has a spatial resolution of about ~10 nm (in ambient);[20,21] whereas, KFM can detect and quantitatively measure the overall contribution of charges including surface charges (chemical species), screen charges, and bound charges of polarization in terms of surface potential. As shown in Figure 2b, the surface potential variation over the ferroelectric domains is mainly governed by the screening charges, which is also the case with SRPM image in Figure 2a.[19,22] However, as KFM detects the electric force with a certain gap between the tip and sample, it has poorer spatial resolution in detecting the ferroelectric domain boundaries than that of PFM.[23] As can be seen from the line profiles shown in Figure 2d, RP has the same or similar spatial resolution as that of PFM phase images and has a capability to detect the screen charges like KFM. Although there is an issue with quantitative estimation of surface charge with RP, we can solve it by calibrating RP with a standard sample used for sensitivity measurement[14] and convert the surface potential into the amount of surface charges. Another method is to use KFM and macroscopic electrical measurement data to evaluate the overall net surface charge over a large area and roughly estimate the net surface charge over a small area. In the case

dx.doi.org/10.1021/nl103372a |Nano Lett. 2011, 11, 1428–1433

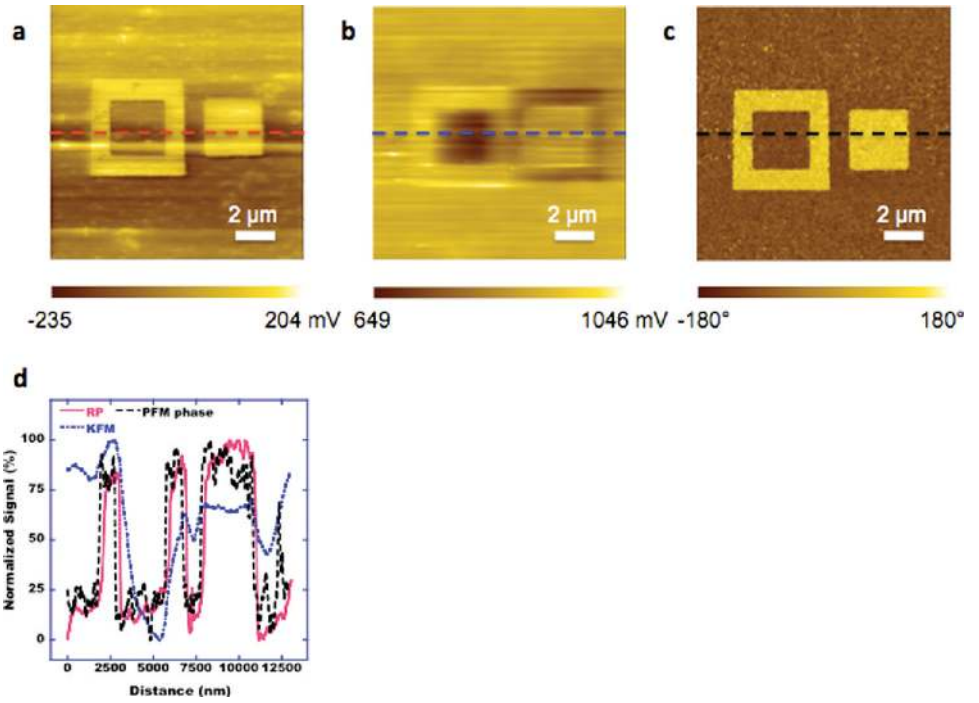

Figure 2. Comparison between SRPM, KFM, and PFM phase images of positively and negatively polarized domains in square patterns. (a−c) SRPM (a), KFM (b), and PFM phase images (c). (d) Line profiles of SRPM (red curve), KFM (blue curve), and PFM phase (black curve) images across the centerlines.

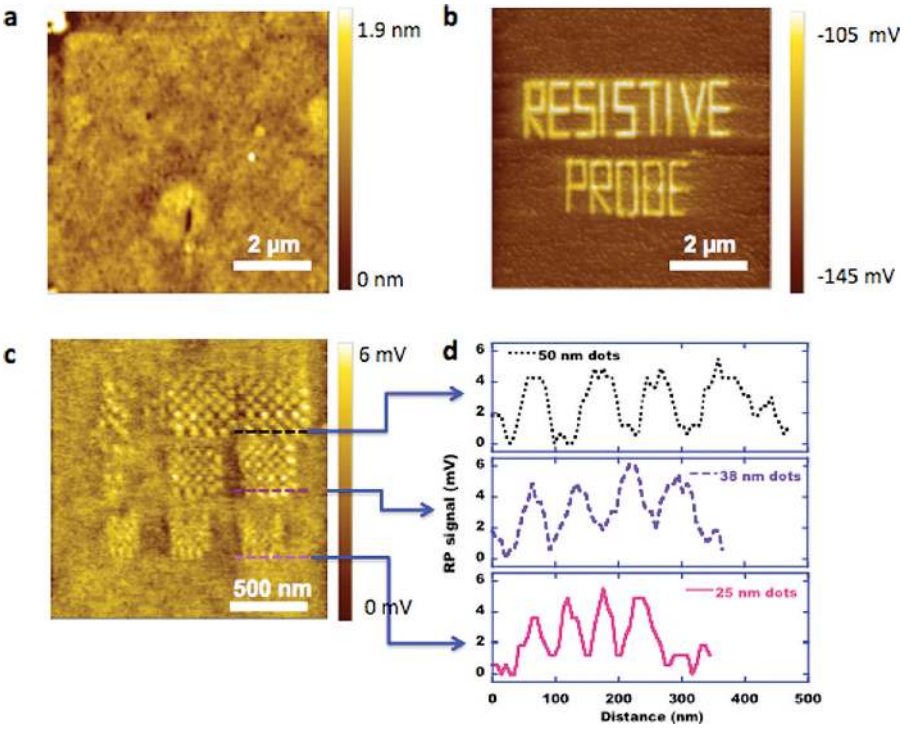

Figure 3. Manipulation and detection of surface charges using SRPM. (a,b) Topography (a) and SRPM (b) images of artificially polarized domains with letters showing "RESISTIVE PROBE". (c,d) Checkerboard patterns of alternating positive and negative domains imaged by SRPM (c) and selected line profiles of domains with distances of 50, 38, and 25 nm (d).

of a 25 nm diameter domain, if we adopt the measured polarization[24] of 80 μC/cm^2 and over screen charge[19] of 1%, we come up with a charge quantity of ~25 electrons, which gives an upper limit estimate of charge resolution for the SRPM.

We demonstrated in Figure 3a,b that RP can detect surface charges artificially decorated by inducing local ferroelectric switching via voltage bias to the probe without a crosstalk from the topography. The words "RESISTIVE PROBE" are clearly

dx.doi.org/10.1021/nl103372a |*Nano Lett.* 2011, 11, 1428–1433

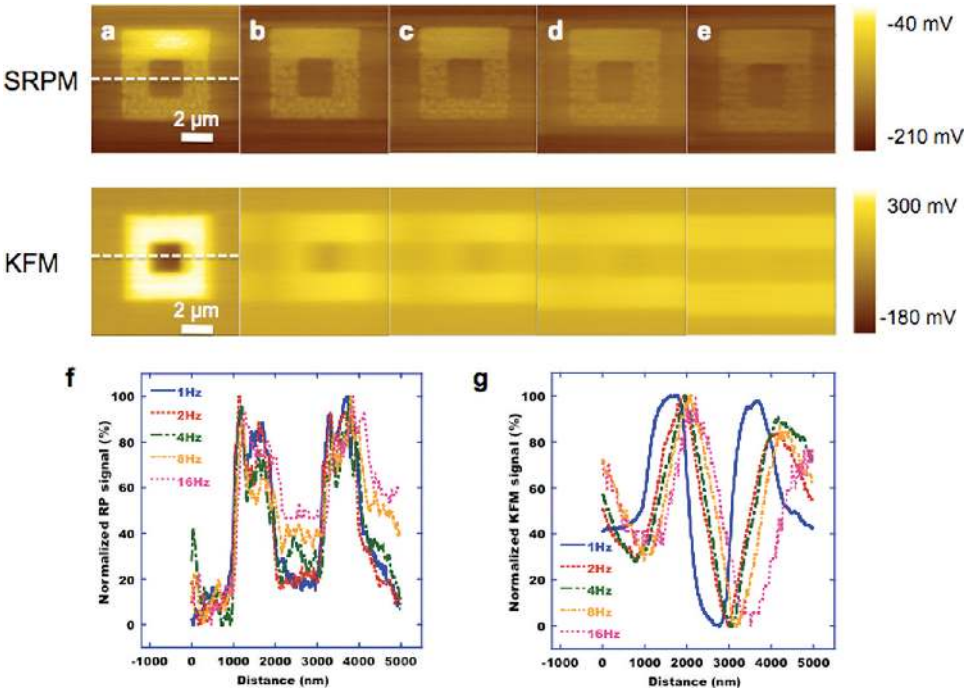

Figure 4. Frequency dependent SRPM and KFM images. (a−e) SRPM (upper row) and KFM images (lower row) at scan frequencies of (a) 1, (b) 2, (c) 4, (d) 8, and (e) 16 Hz. (f, g) Plots of line profiles at centerlines of (f) SRPM and (g) KFM images.

seen in SRPM image (see Figure 3b) without distorting the topography image (see Figure 3a). Equally important is that the surface features of humps and troughs observed in topography is not seen in SRPM image. Furthermore, to study the spatial resolution of RP, we formed checkerboard patterns of various sizes by alternating up and down polarization domains. As shown in Figure 3c and the line profiles across the patterns, we could distinguish domains of less than 25 nm in diameter. This is more than 8 times improvement of resolution as compared with our previous record reported elsewhere[15] and is close to that of PFM.[20] Furthermore, RP can potentially operate at >100 MHz due to its ultrafast response time (<10 ns),[15] which is feasible with neither PFM nor KFM.[25] Therefore, we believe that RP can be used as a high-density information storage reader in ferroelectric-based storage devices.[15,26−28]

Although RP has a response time of less than 10 ns, in practice the scanner in atomic force microscopy (AFM) will limit the rate of RP image acquisition. Figure 4 illustrates the high-speed capability of RP and its comparison with KFM. We scanned the RP tip from 1 up to 16 Hz and then reduced the scan speed back to 1 Hz whereas we started from 0.25 up to 16 Hz and returned to 0.25 Hz in KFM. To compare SRPM and KFM on one-to-one basis, we chose scan frequencies of 1, 2, 4, 8, and 16 Hz in Figure 4a−e. As expected from our previous response time measurement of RPs,[15] we observed another great advantage of SRPM over KFM in that the spatial resolution of SRPM is persistent as we increase the scan rate at least up to 16 Hz, whereas the KFM images become rather unreliable when the scan rate exceeded 2 Hz. Since one scan line consists of 256 pixels, the residence time over a pixel at the scan rate of 16 Hz is ~125 μs, which provides the upper limit of temporal resolution in SRPM. However, it should be noted that the absolute amount of surface charge changes because they can drain into the RP tip as is the case with grounded conductive tip.[19,29] The topography, SRPM and KFM images remained the same when we return to the original scan rate (1 Hz for SRPM and 0.25 Hz for KFM).

In summary, we have developed a novel probe that can directly image the surface potential or charge by a conventional AFM without a lock-in amplifier. Spatial resolution of less than 25 nm and temporal resolution below 125 μs (with a potential below 10 ns) have been demonstrated, which combines the advantages of KFM (or EFM) and PFM with higher speeds. On the basis of the comparative images between KFM and RP and the fact that PFM cannot detect surface charges, one can immediately recognize the advantage of using RP over KFM and PFM: direct measurement of the surface potential with higher spatial and temporal resolutions. The types of scientific questions that could be answered by this technique include nanoscale polarization-switching dynamics at or close to the physical limit of its switching time of ferroelectric thin films, fast relaxation mechanism of charges trapped in oxide or ferroic nanostructures, and in vitro/in vivo observation of charge transport in bone or neuron cells. Thus, this probing technique will be beneficial not only for condensed matter research and relevant applications, but also for soft matter study, for example, biophysics where one can get surface charge information decoupled from mechanical damping of the cantilevers in liquid environment.

Methods and Materials. *Fabrication of Resistive Probes.* We used silicon on insulator (SOI) wafers, as the starting material where an 800 nm thick oxide layer was thermally grown on a 6 μm thick p-type ($1 \times 10^{15}/cm^3$) device layer. The oxide layer was patterned to define source and drain regions and used as masks for ion implantation (As^{2+}, acceleration energy of 150 keV, and dose of $1 \times 10^{16}/cm^2$). After the ion implantation, annealing process for dopant activation and diffusion was conducted at 1000 °C for 12 h under dry N_2 environment. During this annealing process, the implanted regions expanded diffusively and the boundaries of implanted regions, where doping concentration was $10^{15}-10^{16}/cm^3$, were eventually overlapped, forming the resistive region under the mask. Subsequently, we patterned the implantation mask layer to form a tip etch mask with various aspect ratios to control the shape of the tip apex (see

dx.doi.org/10.1021/nl103372a |*Nano Lett.* 2011, 11, 1428–1433

Supporting Information). RP tip was formed by an isotropic Si wet etching in HNA (hydrofluoric nitric−acetic) solution, followed by sharpening oxidation process. More detailed fabrication process of RP can be found elsewhere.[30]

Preparation of Ferroelectric Thin Films. Highly polar $PbZr_{0.2}Ti_{0.8}O_3$ (P_r = 80 $\mu C/cm^2$) epitaxial thin films have been grown by pulsed laser deposition (PLD) on atomically flat, conducting $SrRuO_3$ films on $SrTiO_3$ single crystal substrates (cubic, a = 0.3905 nm). Details on the thin film synthesis, structures, and ferroelectric properties can be found elsewhere.[24]

Process and Device Simulation. We conducted the process simulation of the resistive probe structure by using ATHENA (Silvaco). The input parameters were As^+ implant energy (300 keV), dose ($1 \times 10^{16}/cm^2$), and incident angle for implantation process, and diffusion time, temperature, lateral diffusivity for both diffusion and oxidation-enhanced diffusion processes. After the diffusion process, we removed the part that was etched in accordance with the experimental data for the tip shape from SEM images. The resulting tip shape with its dopant profile was fed into the device simulator (ATLAS, Silvaco). With these input parameters, we calculated the sensitivity and spatial resolution as described in ref 17 (see Supporting Information for more details).

PFM and KFM Characterization. We first poled the sample top-down (negative direction) by applying −8 V to the bottom electrode over the area of 3 × 3 μm^2. Then we applied +8 V inside the negatively poled area over 1 × 1 μm^2. As shown in Figure 3, we formed another box pattern by reversing the polarity of voltage applied to the bottom electrode, that is, applying +8 V over 3 × 3 μm^2 and subsequently applying −8 V over 1 × 1 μm^2. For PFM image acquisition,[31] we used Pt-coated Si tips (NSG01-Pt, spring constant: 5.5 N/m, NT-MDT, Inc.) and connected the lock-in amplifier (SR 830, Stanford Research Systems) to the SPM (SPM 400, SII, Japan) unit. The reference amplitude and frequency of the modulation signal generated by the lock-in amplifier were 0.8 V_{rms} and 17 kHz. We used a phase offset of −90° to keep the PFM phase values between −90° and 90°. The scan frequency was 0.7 Hz. For KFM, we used Au-coated Si tips (DF3-A, spring constant, 1.6 N/m; resonance frequency, 24 kHz; SII, Japan) and applied 6 V_{pp} ac modulation voltage at 14.4 kHz to the tip. The scan frequency was 0.2 Hz for Figure 3b and was varied from 1 to 16 Hz for Figure 4.

■ ASSOCIATED CONTENT

Supporting Information. Methods and materials, additional figures, table, and references. This material is available free of charge via the Internet at http://pubs.acs.org.

■ AUTHOR INFORMATION

Corresponding Author
*E-mail: hong@anl.gov.

■ ACKNOWLEDGMENT

The main part of this work was supported by Samsung Electronics, Inc. S.H. acknowledges financial support by U Chicago Argonne, a U.S. DOE Office of Science Laboratory, operated under Contract no. DE-AC02-06CH11357. H.S. acknowledges financial supports from the NRL program (2007-0057024), the Nano R&D program (2009-0082717), the CMPS (R11-2005-048-00000-0) of Korean NRF and the 2009 research program of Kookmin University. The Work at Oak Ridge National Laboratory (H.N.L.) was sponsored by the Materials Science and Engineering Division, Office of Basic Energy Sciences, U.S. Department of Energy. We gratefully acknowledge G. Crabtree at Argonne National Laboratory for his critical reading of this manuscript. H.K., H.P., H.S. and S.H. conceived the wedge-shaped resistive probe experiments, conducted the data analysis, and wrote the paper. H.K., H.P., C.P., D.M., D.J., and Y.P. designed, fabricated, and characterized the resistive probes, J. J. and H.K. carried out TCAD simulation of the proposed RP design, and K.R., S.H., and Y.K. performed the comparison studies of PFM, KFM, and RP. H.K. and K.R. conducted the high speed RP measurement. Y.K.K. and H.N.L. provided epitaxial PZT samples and discussed the data acquired by PFM, KFM, and RP.

■ REFERENCES

(1) Nonnenmacher, M.; O'Boyle, M. P.; Wickramasinghe, H. K. Kelvin probe force microscopy. *Appl. Phys. Lett.* **1991**, *88*, 2921–2923.
(2) Hehn, M.; Ounadjela, K.; Bucher, J.-P.; Rousseaux, F.; Decanini, D.; Bartenlian, B.; Chappert, C. Nanoscale magnetic domains in mesoscopic magnets. *Science* **1996**, *272*, 1782–1785.
(3) Sugimoto, Y.; Pou, P.; Abe, M.; Jelinek, P.; Perez, R.; Morita, S.; Custance, O. Chemical identification of individual surface atoms by atomic force microscopy. *Nature* **2007**, *446*, 64–67.
(4) Balke, N.; Choudhury, S.; Jesse, S.; Huijben, M.; Chu, Y. H.; Baddorf, A. P.; Chen, L. Q.; Ramesh, R.; Kalinin, S. V. Deterministic control of ferroelastic switching in multiferroic materials. *Nat. Nanotechnol.* **2009**, *4*, 868–875.
(5) Majumdar, A. Scanning thermal microscopy. *Annu. Rev. Mater. Sci.* **1999**, *29*, 505–585.
(6) Kalinin, S. V.; Bonnell, D. A.; Alvarez, T.; Lei, X.; Hu, Z.; Shao, R.; Ferris, J. H. Ferroelectric Lithography of Multicomponent Nanostructures. *Adv. Mater.* **2004**, *16*, 795–799.
(7) Vettiger, P.; Cross, G.; Despont, M.; Drechsler, U.; Durig, U.; Gotsmann, B.; Haberle, W.; Lantz, M. A.; Rothuizen, H. E.; Stutz, R.; Binnig, G. K. The "millipede"- nanotechnology entering data storage. *IEEE Trans. Nanotechnol.* **2002**, *1*, 39–55.
(8) Ahn, C. H.; Rabe, K. M.; Triscone, J-. M. Ferroelectricity at the Nanoscale: Local Polarization in Oxide Thin Films and Heterostructures. *Science* **1997**, *276*, 1100–1103.
(9) Sinensky, A. K.; Belcher, A. M. Label-free and high-resolution protein/DNA nanoarray analysis using Kelvin probe force microscopy. *Nat. Nanotechnol.* **2007**, *2*, 653–659.
(10) Cui, X.; Freitag, M.; Martel, R.; Brus, L.; Avouris, P. Controlling energy-level alignments at carbon nanotube/Au contacts. *Nano Lett.* **2003**, *3*, 735–740.
(11) Coffey, D. C.; Ginger, D. S. Time-resolved electrostatic force microscopy of polymer solar cells. *Nat. Mater.* **2006**, *5*, 735–740.
(12) Yoo, M. J.; Fulton, T. A.; Hess, H. F.; Willett, R. L.; Dunkleberger, L. N.; Chichester, R. J.; Pfeiffer, L. N.; West, K. W. Scanning Single-Electron Transistor Microscopy: Imaging Individual Charges. *Science* **1997**, *276*, 579–582.
(13) Suh, M. S.; Choi, J. H.; Kuk, Y.; Jung, J. Silicon-based field-effect-transistor cantilever for surface potential mapping. *Appl. Phys. Lett.* **2003**, *83*, 386–388.
(14) Park, H.; Jung, J.; Min, D.-K.; Kim, S.; Hong, S.; Shin, H. Scanning resistive probe microscopy: Imaging ferroelectric domains. *Appl. Phys. Lett.* **2004**, *84*, 1734–1736.
(15) Hong, S.; Park, N. Resistive Probe Storage: Read/Write Mechanism. In *Scanning Probe Microscopy: Electrical and Electromechanical Phenomena at the Nanoscale*; Kalinin, S. V., Gruverman, A., Eds.; Springer: New York, 2006; Vol. 2, pp 943−973.
(16) See, for example, http://en.wikipedia.org/wiki/Technology_CAD. Accessed November 13, 2009.
(17) Kim, J.; Lee, J.; Song, I.; Lee, J. D.; Park, B. -G.; Hong, S.; Ko, H.; Min, D. −K.; Park, H.; Park, C.; Jung, J.; Shin, H. Characterization of Sensitivity and Resolution of Silicon Resistive Probe. *Jpn. J. Appl. Phys.* **2008**, *47*, 1717–1722.

(18) Shin, H.; Kim, C.; Lee, B.; Lee, J.; Park, H.; Min, D.-K.; Jung, J.; Hong, S.; Kim, S. Formation and process optimization of scanning resistive probe. *J. Vac. Sci. Technol., B* **2006**, *24*, 2417–2420.

(19) Kim, Y.; Bae, C.; Ryu, K.; Ko, H.; Kim, Y. K.; Hong, S.; Shin, H. Origin of surface potential change during ferroelectric switching in epitaxial $PbTiO_3$ thin films studied by scanning force microscopy. *Appl. Phys. Lett.* **2009**, *94*, No. 032907.

(20) Rodriguez, B. J.; Jesse, S.; Baddorf, A. P.; Kalinin, S. V. High resolution electromechanical imaging of ferroelectric materials in a liquid environment by piezoresponse force microscopy. *Phys. Rev. Lett.* **2006**, *96*, No. 237602.

(21) Kalinin, S. V.; Jesse, S.; Rodriguez, B. J.; Shin, J.; Baddorf, A. P.; Lee, H. N.; Borisevich, A.; Pennycook, S. J. Spatial resolution, information limit, and contrast transfer in piezoresponse force microscopy. *Nanotechnology* **2006**, *17*, 3400–3411.

(22) Kalinin, S. V.; Bonnell, D. A. Polarization and Charge Dynamics in Ferroelectric Materials with SPM. In *Nanoscale Phenomena in Ferroelectric Thin Films*; Hong, S., Ed.; Kluwer Academic Publisher: Boston, 2004; Chapter 8, pp 183−217.

(23) Jacobs, H. O.; Leuchtmann, P.; Homan, O. J.; Stemmer, A. Resolution and contrast in Kelvin probe force microscopy. *J. Appl. Phys.* **1998**, *84*, 1168–1173.

(24) Lee, H. N.; Nakhmanson, S. M.; Chisholm, M. F.; Christen, H. M.; Rabe, K. M.; Vanderbilt, D. Suppressed dependence of polarization on epitaxial strain in highly polar ferroelectrics. *Phys. Rev. Lett.* **2007**, *98*, No. 217602.

(25) Nath, R.; Chu, Y.-H.; Polomoff, N. A.; Ramesh, R.; Huey, B. D. High speed piezoresponse force microscopy: < 1 frame per second nanoscale imaging. *Appl. Phys. Lett.* **2008**, *93*, No. 072905.

(26) Tanaka, K.; Kurihashi, Y.; Uda, T.; Daimon, Y.; Odagawa, N.; Hirose, R.; Hiranaga, Y.; Cho, Y. Scanning Nonlinear Dielectric Microscopy Nano-Science and Technology for Next Generation High Density Ferroelectric Data Storage. *Jpn. J. Appl. Phys.* **2008**, *47*, 3311–3325.

(27) Ahn, C. H.; Rabe, K. M.; Triscone, J. M. Ferroelectricity at the Nanoscale: Local Polarization in Oxide Thin Films and Heterostructures. *Science* **2004**, *303*, 488–491.

(28) Waser, R.; Rüdiger, A. Ferroelectrics: Pushing towards the digital storage limit. *Nat. Mater.* **2004**, *3*, 81–82.

(29) Kim, Y.; Kim, J.; Bühlmann, S.; Hong, S.; Kim, Y. K.; Kim, S.-H.; No, K. Screen charge transfer by grounded tip on ferroelectric surfaces. *Phys. Status Solidi RRL* **2008**, *2*, 74–76.

(30) Park, H.-S.; Jung, J.-H.; Hong, S.-B. Method of fabricating semiconductor probe with resistive tip. U.S. Patent 7,338,831, 2008.

(31) Hong, S.; Woo, J.; Shin, H.; Jeon, J. U.; Pak, Y. E.; Colla, E. L.; Setter, N.; Kim, E.; No, K. Principle of Ferroelectric Domain Imaging using Atomic Force Microscope. *J. Appl. Phys.* **2001**, *89*, 1377–1386.